LEVEL SET-BASED TRACKING OF THE ENDOCARDIUM WITHOUT A SHAPE PRIOR FROM 3D ULTRASOUND IMAGES

Yrjö Häme[⋆]*, Viktor Gamarnik*[⋆]*, Katherine M. Parker*[†]*, Jeffrey W. Holmes*[†]*, Andrew F. Laine*[⋆]

[⋆] Department of Biomedical Engineering, Columbia University, New York, NY, USA
[†]Department of Biomedical Engineering, University of Virginia, Charlottesville, VA, USA

ABSTRACT

A level set-based method for tracking the endocardium from 3D ultrasound images is presented. The tracking process is initialized by a manual delineation and performed automatically. The method does not use a shape prior model, removing the requirement of acquiring large sets of training data, and providing adaptivity for abnormal cases. At each image frame, the edge strength is estimated and locations with strong edges are used to compute the region-based surface deformation, which is then propagated to the rest of the image volume. The approach is evaluated with 10 sequences of canine subjects including 5 ischemic image sequences. The results show that the method performs with error values below the interobserver variability of manual segmentation, and is able to robustly follow the cardiac wall movement.

Index Terms— tracking, 3D echocardiography, level set methods

1. INTRODUCTION

Even with the constant introduction of new cardiac imaging techniques, echocardiography remains the mainstay of clinical diagnosis of various cardiac diseases including heart failure [1], coronary vessel disease (via stress echo) [2], conduction abnormalities such as bundle branch blocks (via tissue doppler/ strain imaging) [3] and various cardiomyopathies. Ease of use and low cost have contributed to the proliferation and importance of 2D echocardiography. Real-time 3D echocardiography (RT3DE) has the potential to not only improve current methods of diagnostic imaging, but also to allow for assessment of parameters that cannot be accurately measured in 2D. Although RT3DE machines have been available for over a decade, 3D echo has not been as widely accepted in the clinical field. Presently, RT3DE is still primarily used for structural (rather than functional) evaluation, i.e. for assessment of congenital heart disease [4]. In the few published studies where RT3DE is used for functional evaluation, i.e. for assessment of mechanical dyssynchrony [5], diagnosis relies on segment-based analysis of simple secondary measures such as "time to minimum systolic volume" calculated from the standard 16-segment LV model. In the realm of post-MI follow-up, RT3DE is also used in a "segmental" nature, with evaluation limited to differential volumetric measurements [6].

We believe that the limitations in application of RT3DE to clinical echocardiography arise from the sparse collection of tools available to clinicians for analyzing the large and complex datasets generated by this powerful technique. Automated tracking of the cardiac wall is a challenging task due to missing edge information, speckle noise, subject variability and variation in intensity distributions. In previous work, shape priors are effectively used [7, 8]. However, shape priors have two major disadvantages: they require a significant amount of training data and they may not be able to cope well with abnormal cases. Other recent work includes methods based on a Kalman filter [9], optical flow [10], and an approach combining structural and textural information [11]. Also, methods based on deformable models have previously been used for segmentation of the endocardium [12, 13].

To assist clinicians in visualizing and interpreting 3D echocardiograms, we propose a technique for automatic tracking of the endocardial wall based on a manual boundary initialization, without using a shape prior. In the present work, we describe the implementation and evaluation of the method in normal as well as ischemic cases.

2. METHODS

2.1. Data Acquisition

The data used in this analysis was acquired from five open chest dogs. The research protocol was approved by Columbia University's Institutional Animal Care and Use Committee. Anaesthesia was induced with propofol and was maintained using inhaled isoflurane. A lateral thoracotomy was performed and the pericardium was opened and sutured to the chest wall to expose the left ventricle. Sutures were placed around the left anterior descending (LAD) and left circumflex (LCx) coronary arteries or their branches at proximal

The imaging studies were funded by grants AHA 0640005N and NIH R01HL08516. Yrjö Häme is funded by the International Fulbright Science and Technology Award at the U.S. Department of State.

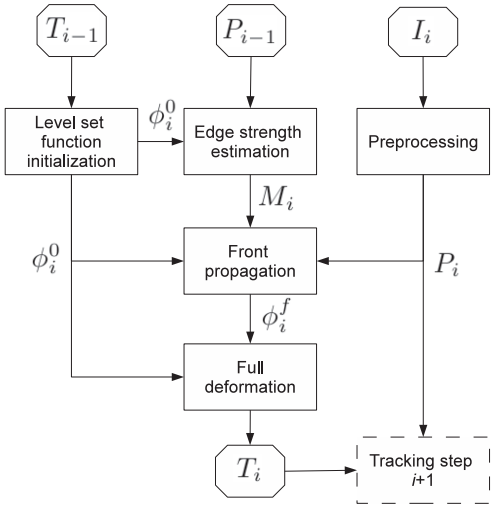


Fig. 1. Stages of the tracking method for step i

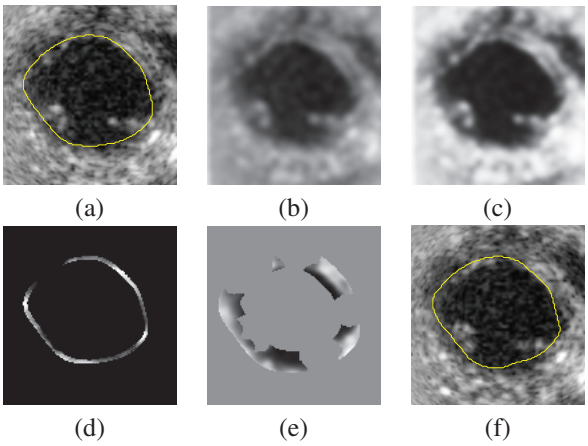


Fig. 2. Illustration of the main stages of the method in a single tracking step: a) Initial boundary T_{i-1} with corresponding image I_{i-1}, b) filtered image I'_{i-1} , c) probability volume P_{i-1}, d) edge strength estimate E_i, e) P_i at narrow band mask M_i, f) tracking result T_i overlaid on I_i

and distal sites. More details on the experimental set-up are available in [14].

The apical RT3D echocardiograms were then acquired using a Philips iE33 ultrasound system (Philips Medical Systems, Andover, MA). A single cardiac cycle consisted of 10-12 frames. To facilitate stable imaging of the region of interest (LV), a silicone gel standoff (Aquaflex, Parker Laboratories, Fairfield, NJ) was placed between the ultrasound probe and the apex of the heart. At the conclusion of the experiment, all dogs were euthanized by injection of pentobarbital sodium and phenytoin.

2.2. Tracking method overview

The tracking method finds strong edges along the boundary of the previous frame, computes the new deformation at these locations, and then extends the deformation. Each tracking step includes five stages: 1) preprocessing of input image, 2) level set function initialization, 3) edge strength estimation, 4) front propagation and 5) computation of full deformation. The stages are represented in Fig. 1. As input, each step i requires the tracking result from the previous step T_{i-1}, probability volume from previous step P_{i-1}, and the new raw image volume I_i. For the first tracking step, $T_{i-1} = T_0$ is the manual delineation, and P_0 is the preprocessing result (see Section 2.3) for image I_0.

2.3. Preprocessing

In the following, $\mathbf{x} \in \Omega$ defines an image point within the image domain Ω. Also, let μ_0 and σ_0^2 represent respective mean intensity and variance of image points inside the initial manually delineated boundary T_0.

At each tracking step i, the new image volume I_i is first filtered $I'_i = G_{\sigma^2}(I_i)$ by a Gaussian kernel G with variance $\sigma^2 = 1.5$ (see Fig 2b). The probability volume P_i is then obtained using the sigmoidal function

$$P_i(\mathbf{x}) = \frac{1}{1 + e^{-\alpha(I'_i(\mathbf{x})-\beta)}} \quad (1)$$

where $\alpha = \omega_\alpha \sigma_0^2$ and $\beta = \mu_0 + \omega_\beta \sigma_0^2$ with empirically chosen scalar weights $\omega_\alpha = 0.05$ and $\omega_\beta = 0.1$. An example of P_i is shown in Fig. 2c.

2.4. Level set function initialization and edge strength estimation

The initial level set function $\phi_i^0 = \phi_i(\mathbf{x}, t = 0)$ is obtained by computing the signed distance function with the fast marching method [15] to the boundary of T_{i-1}. The edge strength E_i in P_{i-1} is then estimated along the zero level set of ϕ_i^0: $E_i(\mathbf{x}) = P_{i-1}(\mathbf{x} + g(\mathbf{x})) - P_{i-1}(\mathbf{x} - g(\mathbf{x}))$, where $g(\mathbf{x}) = \nabla\phi_i^0(\mathbf{x})/||\nabla\phi_i^0(\mathbf{x})||$ with ∇ being the gradient operator. An instance of the edge strength estimate is shown in Fig. 2d.

The narrow band mask M_i is then constructed for defining which parts of the image have a strong edge and can be used for front propagation:

$$M_i(\mathbf{x}) = \begin{cases} 1 & \mathbf{x} \in \mathbf{x}_E + a\nabla\phi_i^0(\mathbf{x}_E)/||\nabla\phi_i^0(\mathbf{x}_E)|| \\ 0 & \text{otherwise,} \end{cases} \quad (2)$$

where $\mathbf{x}_E = \{\mathbf{x}|E_i(\mathbf{x}) > 0.3\}$ and $-d_{nb} < a < d_{nb}$, d_{nb} being the narrow band width, which has to be sufficiently large to include the cardiac wall deformation in one frame. An example of the mask M_i together with the corresponding values of P_i within M_i are shown in Fig. 2e.

2.5. Front propagation and full deformation

The propagation of the front is prescribed by the standard partial differential equation for level set methods [16]:

$$\phi_t(\mathbf{x},t) = P_i(\mathbf{x})||\nabla\phi(\mathbf{x},t)|| + \omega_\kappa\kappa(\mathbf{x},t)||\nabla\phi(\mathbf{x},t)|| \quad (3)$$

where $\kappa(\mathbf{x},t)$ is the mean curvature of the interface [15], and $\omega_\kappa = -0.15$ is a weight for balancing the influence of the curvature term. The front propagation is performed only within the narrow band M_i, and the output is denoted as ϕ_i^f.

For the last stage, we define a deformation field $D_i(\mathbf{x}_M) = \phi_i^f(\mathbf{x}_M) - \phi_i^0(\mathbf{x}_M)$ for $\mathbf{x}_M = \{\mathbf{x}|M_i(\mathbf{x}) = 1\}$. Then this deformation is extended for other points $\mathbf{x}_O$

$$D_i^f(\mathbf{x}_O) = \mu(D_i[\mathbf{x}_M \in N(\mathbf{x}_O)]), \quad (4)$$

where μ denotes the mean and $N(\mathbf{x}_O)$ defines the neighborhood of $\mathbf{x}_O$ as all the points on the axial slices within 1 mm of the axial slice of $\mathbf{x}_O$. The final delineation T_i is given by the zero level set of $G_{\sigma^2}(\phi_i^0 + D_i^f)$, where $\sigma^2 = 3.5$. For lower quality data, the neighborhood size should be increased to keep the interface moving at possible large gaps in M_i.

3. RESULTS

3.1. Data and evaluation measures

The evaluation data consisted of 5 canine subjects with two sequences each, a baseline sequence and another obtained after ischemia induced via occlusion of the LAD or LCx. For each sequence, manual delineations by two clinicians were available, at the end diastolic and end systolic phases.

The tracking method was initialized with one of the manual delineations in the end diastolic phase. Tracking was performed until end systole, with the sequence including 6 or 7 image frames in total, depending on the subject. The tracking result was then evaluated against the corresponding manual delineation of the same observer as the initialization. The delineation by the other observer was used to quantify interobserver variability. The delineations were compared with the following five measures [17]: i) volumetric overlap error [%] (OE), ii) relative absolute volume difference [%] (VD), iii) average symmetric surface distance [mm] (SD), iv) root mean square (RMS) symmetric surface distance [mm] (RD), and v) maximum symmetric surface distance [mm] (MD).

3.2. Evaluation results

The results for baseline images and ischemic images are presented in Tables 1 and 2 respectively. An example of a result is shown in Fig. 3.

The mean overlap error values, 18.23% for baseline images and 22.54% for ischemic images show that the method achieves high accuracy, and the error values of the developed tracking method are consistently smaller than the interobserver variability. For example, the mean overlap error of the method is 8 percentage points smaller for baseline images and almost 6 percentage points smaller for ischemic images than interobserver variability. The robustness of the method is evident from the lack of significant errors in the automatic tracking results, with worst overlap error being 21.15% for baseline and 28.21% for ischemic, and worst maximum surface distance being 6.31 mm for baseline and 6.41 mm for ischemic cases. It is noted that the two observers disagreed especially for one delineation where the volume difference and overlap difference were close to 40%.

Table 1. Evaluation results for baseline images, for presented automatic method (*Aut.*) and interobserver variability (*Inter.*)

		OE	VD	SD	RD	MD
Aut.	Mean	18.23	8.58	0.98	1.30	4.80
	SD	2.12	4.60	0.10	0.15	0.87
	Worst	21.15	16.12	1.14	1.52	6.31
	Best	15.39	4.59	0.86	1.11	4.15
Inter.	Mean	26.27	18.87	1.52	1.88	6.13
	SD	9.26	14.79	0.73	0.78	1.51
	Worst	39.91	39.66	2.60	3.04	8.39
	Best	19.67	6.14	1.02	1.35	5.23

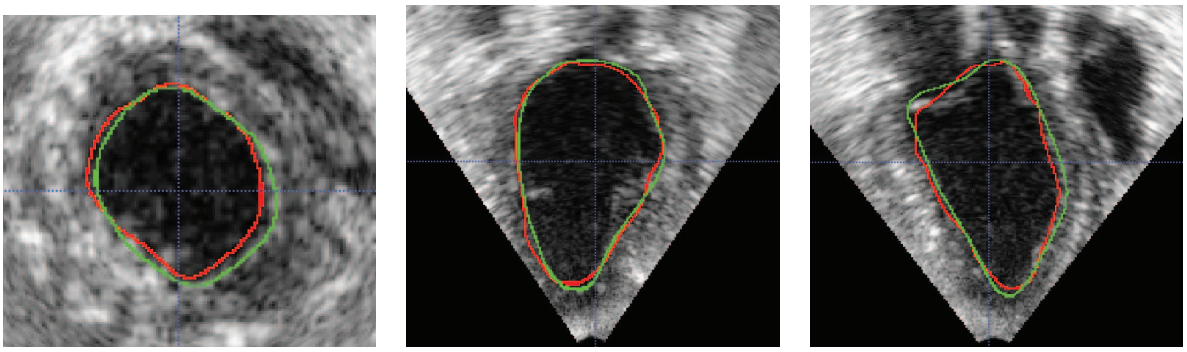
Table 2. Evaluation results for ischemic images, for presented automatic method (*Aut.*) and interobserver variability (*Inter.*)

		OE	VD	SD	RD	MD
Aut.	Mean	22.54	13.68	1.29	1.64	5.39
	SD	4.04	8.50	0.33	0.36	0.84
	Worst	28.21	26.74	1.63	2.00	6.41
	Best	18.10	2.94	0.86	1.14	4.43
Inter.	Mean	28.37	24.98	1.69	2.16	7.71
	SD	7.79	9.87	0.66	0.68	0.99
	Worst	39.97	39.70	2.76	3.27	9.48
	Best	21.13	16.16	1.20	1.56	7.18

The mean symmetric surface distance and maximum distance values (0.98 mm and 4.80 mm for baseline, 1.29 mm and 5.39 mm for ischemic) show that the surface of the tracking result is close to the manually delineated surface. The error values and the interobserver variability are slightly higher for the ischemic images than for the baseline images.

4. DISCUSSION

The accuracy of the technique was demonstrated to be higher than the range of interobserver variability, while providing a significant advantage in terms of time and objective quantification of data at much higher resolutions than afforded by segmental LV models. The average and maximum surface distance values show that the surface produced by the tracking method can be reliably used for quantification of cardiac wall motion.



(a) (b) (c)

Fig. 3. Example of baseline image tracking result in the end systolic phase after 7 frames, with automatic tracking result in red and manual reference delineation in green.

5. REFERENCES

[1] F.D.R. Hobbs, J. Doust, J. Mant, and M.R. Cowie, "Heart failure: Diagnosis of Heart Failure in Primary Care," *Heart*, vol. 96, no. 21, pp. 1773–1777, 2010.

[2] N. Mahajan, L. Polavaram, H. Vankayala, B. Ference, Y. Wang, J. Ager, J. Kovach, and L. Afonso, "Diagnostic Accuracy of Myocardial Perfusion Imaging and Stress Echocardiography for the Diagnosis of Left Main and Triple Vessel Coronary Artery Disease: a Comparative Meta-Analysis," *Heart*, vol. 96, no. 12, pp. 956–966, 2010.

[3] C. Miyazaki, B.D. Powell, C.J. Bruce, R.E. Espinosa, M.M. Redfield, F.A. Miller, D.L. Hayes, Y.M. Cha, and J.K. Oh, "Comparison of Echocardiographic Dyssynchrony Assessment by Tissue Velocity and Strain Imaging in Subjects With or Without Systolic Dysfunction and With or Without Left Bundle-Branch Block," *Circulation*, vol. 117, no. 20, pp. 2617–2625, 2008.

[4] F.G. Hage, S. Raslan, P. Dean, and N.C. Nanda, "Real Time Three-Dimensional Transthoracic Echocardiography in Congenital Heart Disease," *Echocardiography*, 2011.

[5] R. Samir, M. Tawfik, A.M. El Missiri, G. El Shahid, M.A. Maaty, and M. El Sayed, "Assessment of Left Ventricular Mechanical Dyssynchrony Using Real Time Three-Dimensional Echocardiography: A Comparative Study to Doppler Tissue Imaging," *Echocardiography*, 2011.

[6] T. Bochenek, K. Wita, Z. Tabor, M. Grabka, L. Krzych, W. Wróbel, A. Berger-Kucza, M. Elżbieciak, A. Doruchowska, and M.T. Gluza, "Value of Speckle Tracking Echocardiography for Prediction of Left Ventricular Remodeling in Patients with ST-Elevation Myocardial Infarction Treated by Primary Percutaneous Intervention," *JASE*, 2011.

[7] N. Paragios, "A level set approach for shape-driven segmentation and tracking of the left ventricle," *IEEE TMI*, vol. 22, no. 6, pp. 773–776, 2003.

[8] L. Yang, B. Georgescu, Y. Zheng, P. Meer, and D. Comaniciu, "3d ultrasound tracking of the left ventricle using one-step forward prediction and data fusion of collaborative trackers," in *IEEE CVPR*, 2008, pp. 1–8.

[9] F. Orderud, J. Hansgård, and S. Rabben, "Real-time tracking of the left ventricle in 3d echocardiography using a state estimation approach," in *MICCAI*. 2007, pp. 858–865, Springer.

[10] Q. Duan, E.D. Angelini, S.L. Herz, C.M. Ingrassia, K.D. Costa, J.W. Holmes, S. Homma, and A.F. Laine, "Region-based endocardium tracking on real-time three-dimensional ultrasound," *Ultrasound in medicine & biology*, vol. 35, no. 2, pp. 256–265, 2009.

[11] A. Myronenko, X. Song, and D.J. Sahn, "Lv motion tracking from 3d echocardiography using textural and structural information," in *MICCAI*. 2007, pp. 428–435, Springer-Verlag.

[12] E.D. Angelini, S. Homma, G. Pearson, J.W. Holmes, and A.F. Laine, "Segmentation of real-time three-dimensional ultrasound for quantification of ventricular function: a clinical study on right and left ventricles," *Ultrasound in medicine & biology*, vol. 31, no. 9, pp. 1143–1158, 2005.

[13] M. Nillesen, R. Lopata, H. Huisman, J. Thijssen, L. Kapusta, and C. de Korte, "3d cardiac segmentation using temporal correlation of radio frequency ultrasound data," in *MICCAI*. 2009, pp. 927–934, Springer-Verlag.

[14] S.L. Herz, T Hasegawa, A.N. Makaryus, K.M. Parker, S. Homma, J. Wang, and J.W. Holmes, "Quantitative Three-Dimensional Wall Motion Analysis Predicts Ischemic Region Size and Location," *Ann Biomed Eng*, vol. 38, no. 4, pp. 1367–1376, 2010.

[15] S. Osher and R.P. Fedkiw, *Level set methods and dynamic implicit surfaces*, vol. 153, Springer-Verlag, 2003.

[16] J.A. Sethian, *Level set methods and fast marching methods: evolving interfaces in computational geometry, fluid mechanics, computer vision, and materials science*, Number 3. Cambridge Univ Pr, 1999.

[17] X. Deng and G. Du, "Editorial: 3D Segmentation in the Clinic: A Grand Challenge II – Liver Tumor Segmentation," *MICCAI Workshop Proceedings*, 2008.